Electronic Supplementary Material (ESI) for Nanoscale Horizons.

Supporting Information

Quantum-sized topological insulator/semimetal enables ultrahigh and broadband saturable absorption

Zhexue Chen[a,b], Xinyu Sui[b,c], Zhangqiang Li[a,b], Yueqi Li[a,b], Xinfeng Liu[b,c], Yong Zhang*[, a,b]

[a] CAS Key Laboratory of Nanosystem and Hierarchical Fabrication, CAS Center for Excellence in Nanoscience, National Center for Nanoscience and Technology, Beijing 100190, P. R. China

[b] University of Chinese Academy of Sciences, Beijing 100049, P. R. China

[c] CAS Key Laboratory of Standardization and Measurement for Nanotechnology, CAS Center for Excellence in Nanoscience, National Center for Nanoscience and Technology, Beijing 100190, P. R. China

* E-mail: zhangyong@nanoctr.cn

Experimental Section

Materials. Bismuth selenide (Bi_2Se_3, 99.99%), Antimony telluride (Sb_2Te_3, 99.96%), Titanium sulfide (TiS_2, 99.9%), tetraethyl orthosilicate (TEOS), N-methyl-2-pyrrolidone (NMP), dimethylformamide (DMF), and tetrahydrofuran (THF) were purchased from Shanghai Macklin Biochemical Co., Ltd. *N*-hexane, acetone, isopropanol (IPA), ethanol, and aqueous ammonia (25-28 wt%) were purchased from Tianjin Yongda Chemical Reagent Co., Ltd. Porous anodic alumina (PAA) (0.02 μm pore size) was purchased from Whatman. All of the materials were used as received. Deionized water was used in the experiments.

Production of the QSs. The production of Bi_2Se_3 QSs, Sb_2Te_3 QSs, and TiS_2 QSs from their bulk layered materials was realized by an all-physical top-down method (i.e., combination of silica-assisted ball-milling, sonication-assisted solvent exfoliation) that has been described in detail in our previous work.[S1]

Fabrication of the QSs-PMMA thin films: The QSs-PMMA hybrid thin films were fabricated through solution processing. In brief, PMMA was dissolved in NMP to form a 400 mg mL^{-1} solution. Meanwhile, the QS powders were dispersed in NMP to form 1 mg mL^{-1} dispersions. Based on the pre-designed loading contents and the as-required constant total weight, the PMMA solution and QS dispersions were mixed by vigorous stirring and sonication. The mixture with known volume was dropped into a PTFE mold (a 8μm thick polyimide film as the releasing layer). After complete removal of the solvent from the evenly spreading mixture by moderate heating (70 ℃) overnight on a hot plate, the QSs-PMMA thin films were obtained.

Characterization: Scanning electron microscopy (SEM) images were acquired using a Hitachi SU8220 microscope. Transmission electron microscopy (TEM) images and high-resolution TEM (HRTEM) images were acquired using an FEI Tecnai F20 U-TWIN microscope operated at 200 kV. Atomic force microscopy (AFM) images were acquired using a Bruker MultiMode 8 AFM using SCANASYST-AIR

cantilevers with a nominal tip radius of 2 nm in a scanasyst mode. Zeta potential measurements were conducted using a Malvern Zetasizer Nano ZS analyzer. X-ray diffraction (XRD) patterns were recorded using D/Max-TTRIII (CBO) with Cu Kα radiation (λ=1.54056 Å). Raman spectra were recorded using a Renishaw inVia Plus spectrometer with a 514 nm laser. X-ray photoelectron spectroscopy (XPS) measurements were conducted using an ESCALAB 250Xi electron spectrometer from VG Scientific with 300 W Al Kα radiation. Ultraviolet-visible (UV-vis) absorption spectra were recorded using a Lambda 950 spectrophotometer from PerkinElmer. The optical bandgaps of various QSs were extracted according to the Tauc plots

$$(\alpha \cdot hv)^n = C(hv - E_g)$$

where α is the diffuse absorption coefficient at wavelength λ, h is the Planck's constant, v is the light frequency, n is 2 or 0.5 for direct and indirect transitions, respectively, C is constant, and E_g is optical bandgap of materials. Photoluminescence (PL) measurements were conducted using a HORIBA FluoroMax+ spectrofluorometer with varying excitation wavelengths. Nonlinear absorption measurements were performed with 100 fs pulses from a Coherent Astrella regenerative amplifier. The laser was operated at 532 nm and 800 nm wavelength with a pulse repetition rate of 1 kHz. All photographs were acquired with a digital camera.

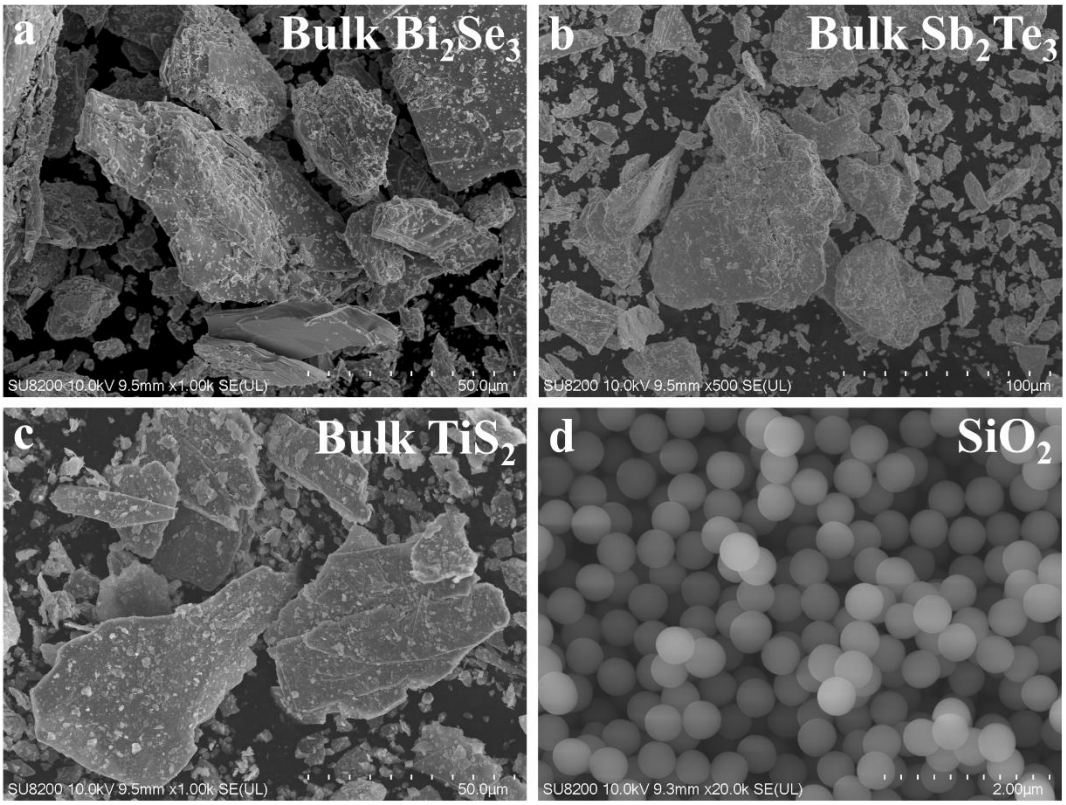

Figure S1. SEM images of bulk layered materials and silica microspheres. (a) Bi_2Se_3, (b) Sb_2Te_3, (c) TiS_2, (d) SiO_2.

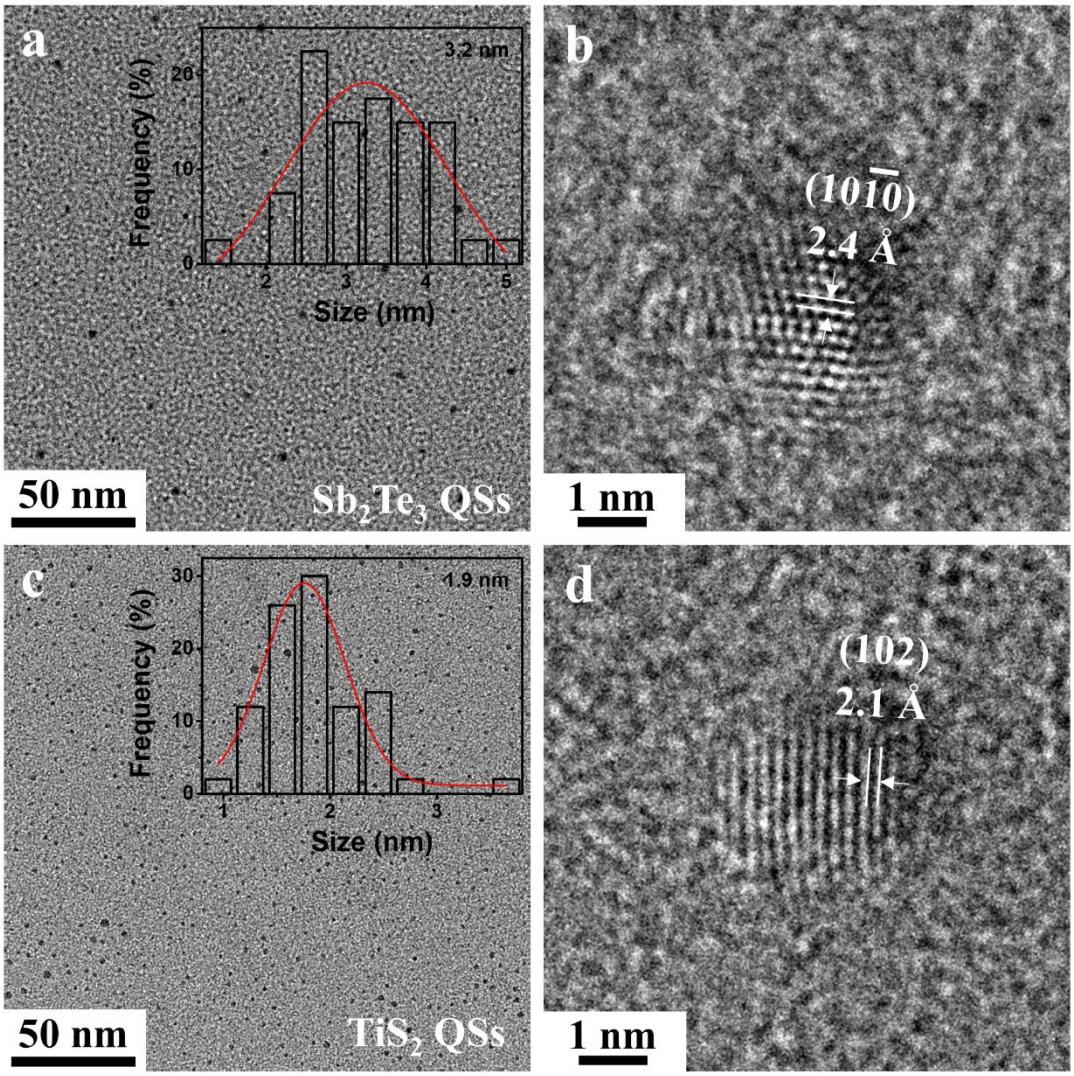

Figure S2. TEM iamges of (a) Sb_2Te_3 QSs and (c) TiS_2 QSs (insets showing the lateral size distributions). HRTEM images of (b) Sb_2Te_3 QSs and (d) TiS_2 QSs.

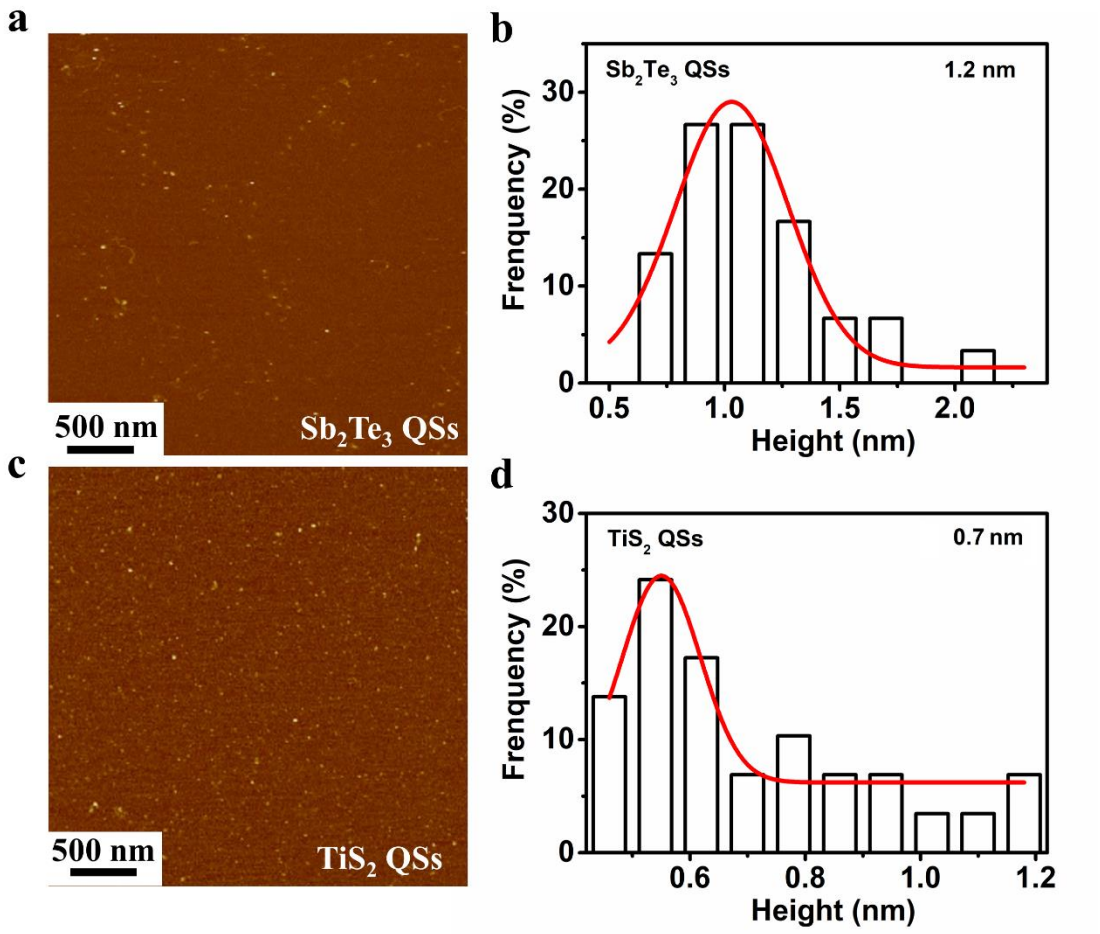

Figure S3. AFM iamges (left) and corresponding height distributions (right) of (a-b) Sb_2Te_3 QSs and (c-d) TiS_2 QSs.

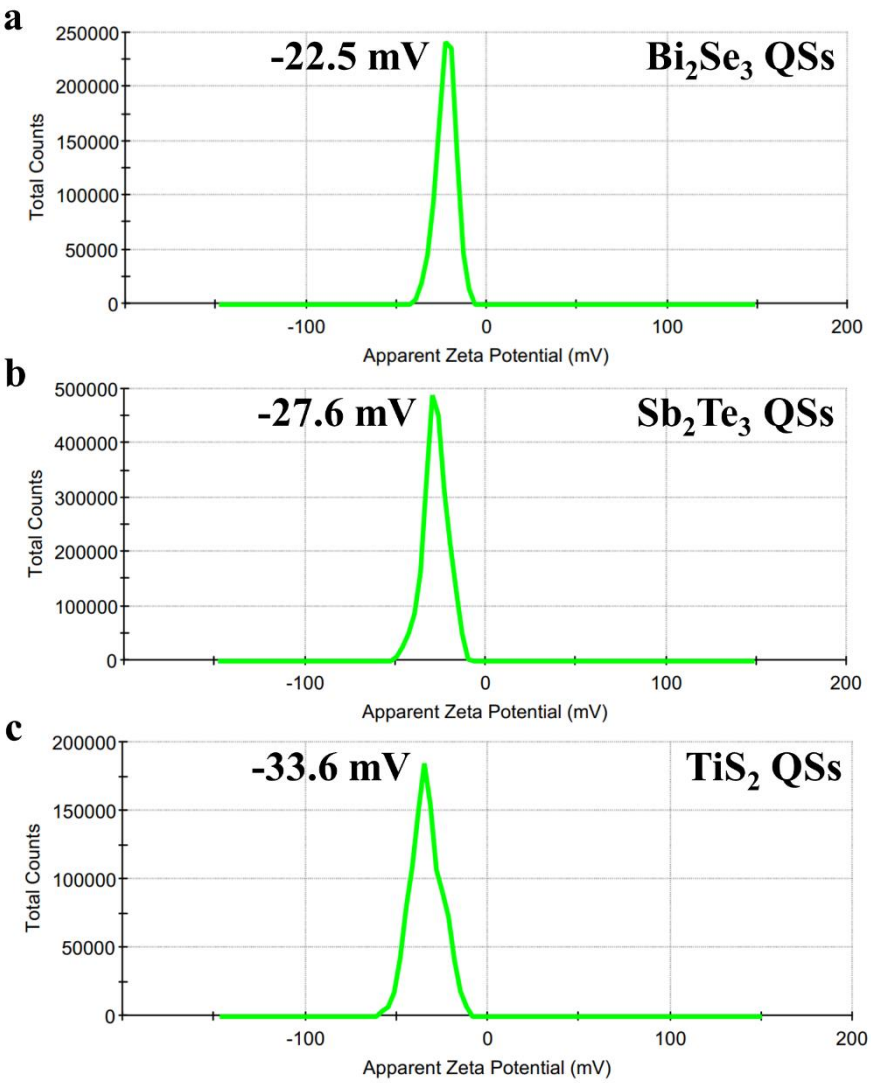

Figure S4. Zeta potentials of the QS aqueous dispersions: (a) Bi_2Se_3 QSs, (b) Sb_2Te_3 QSs and (c) TiS_2 QSs, respectively. The concentration for each dispersion is fixed at 0.1 mg mL^{-1}.

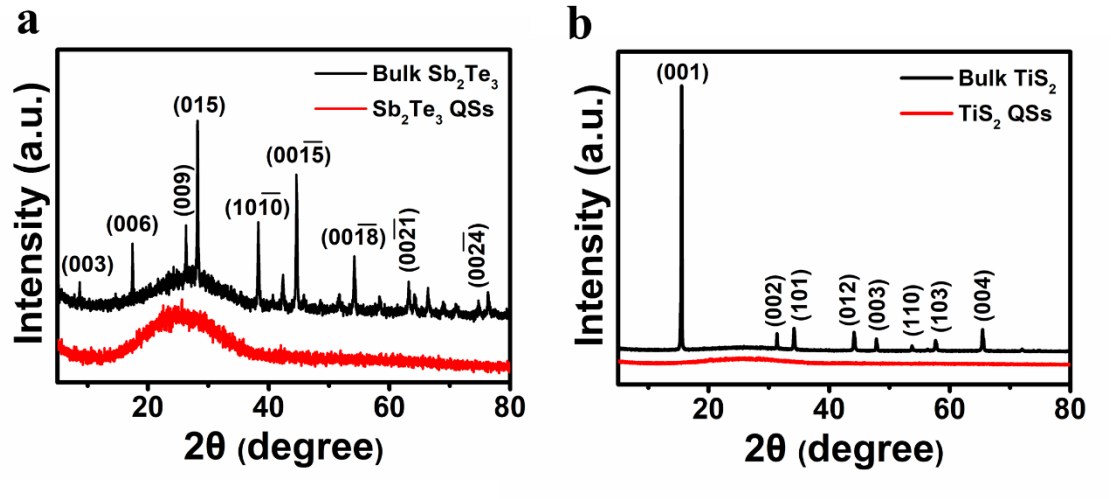

Figure S5. XRD patterns of (a) Sb_2Te_3 QSs and (b) TiS_2 QSs. Data for bulk materials are shown for comparison.

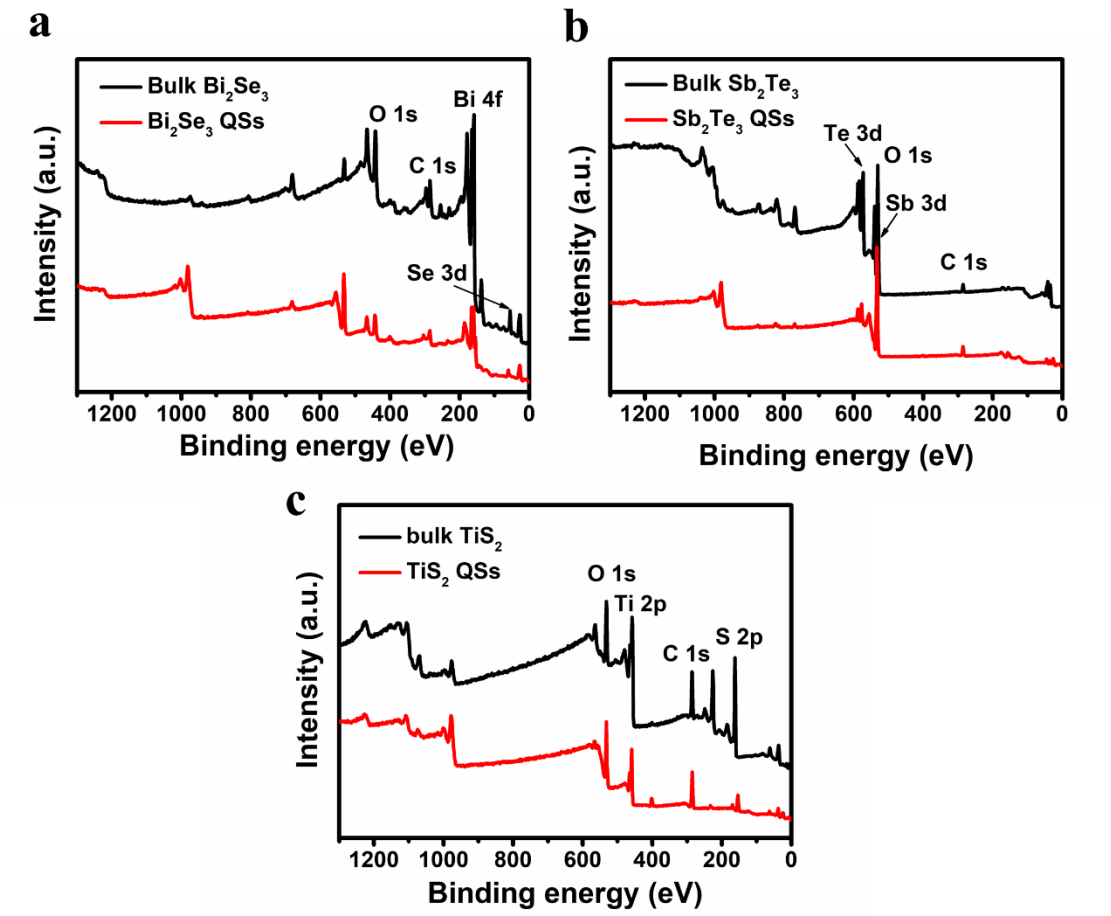

Figure S6. XPS full spectra of (a) Bi_2Se_3 QSs, (b) Sb_2Te_3 QSs and (c) TiS_2 QSs, respectively. Data for bulk materials are shown for comparison.

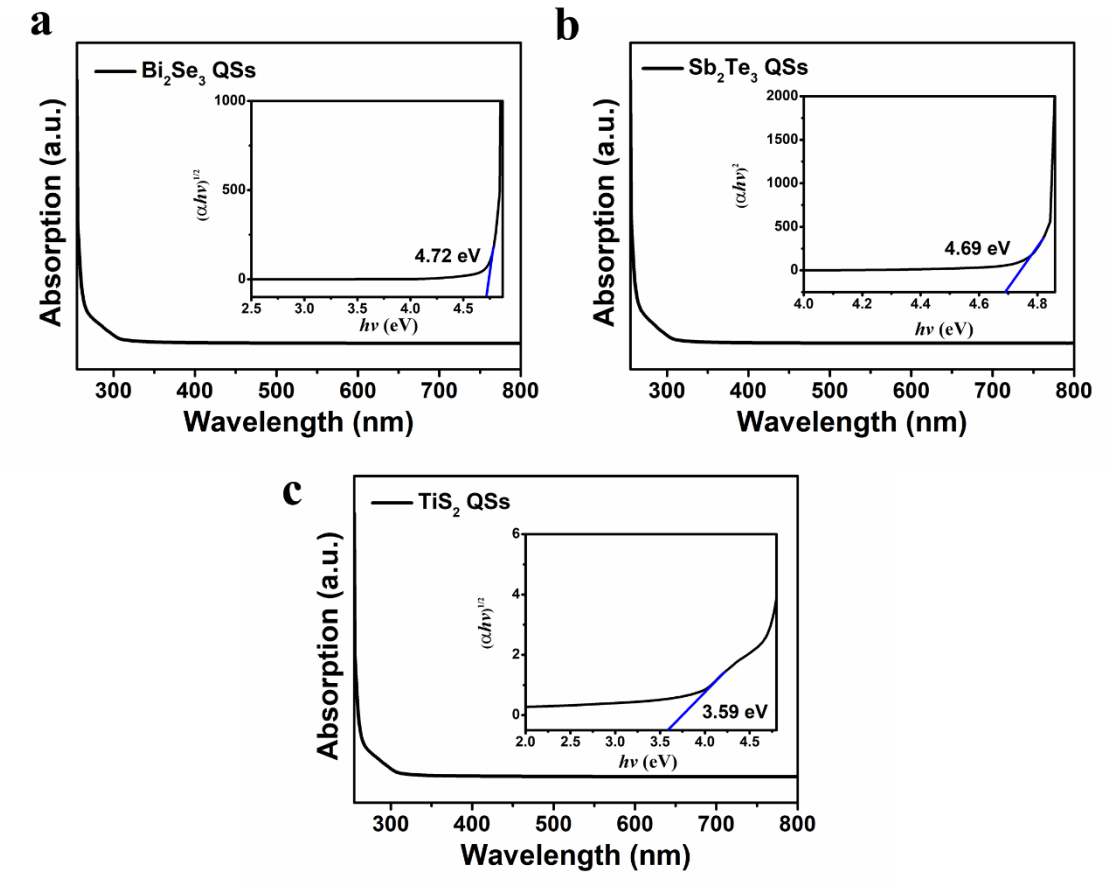

Figure S7. UV-vis absorption spectra (QS/NMP, 0.01 mg mL^{-1}) (insets showing the Tauc analyses) of (a) Bi_2Se_3 QSs, (b) Sb_2Te_3 QSs and (c) TiS_2 QSs, respectively.

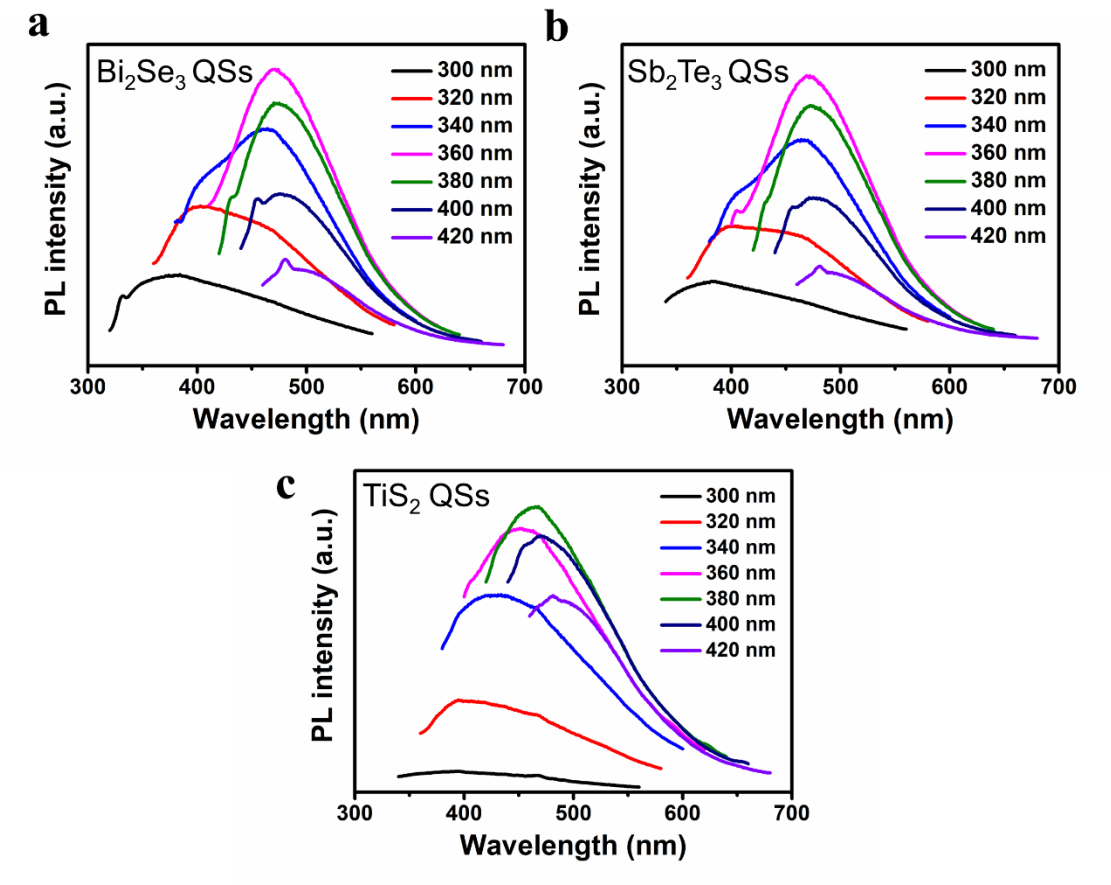

Figure S8. PL spectra of the QS/NMP dispersions at varying excitation wavelengths. (a) Bi_2Se_3 QSs, (b) Sb_2Te_3 QSs and (c) TiS_2 QSs, respectively.

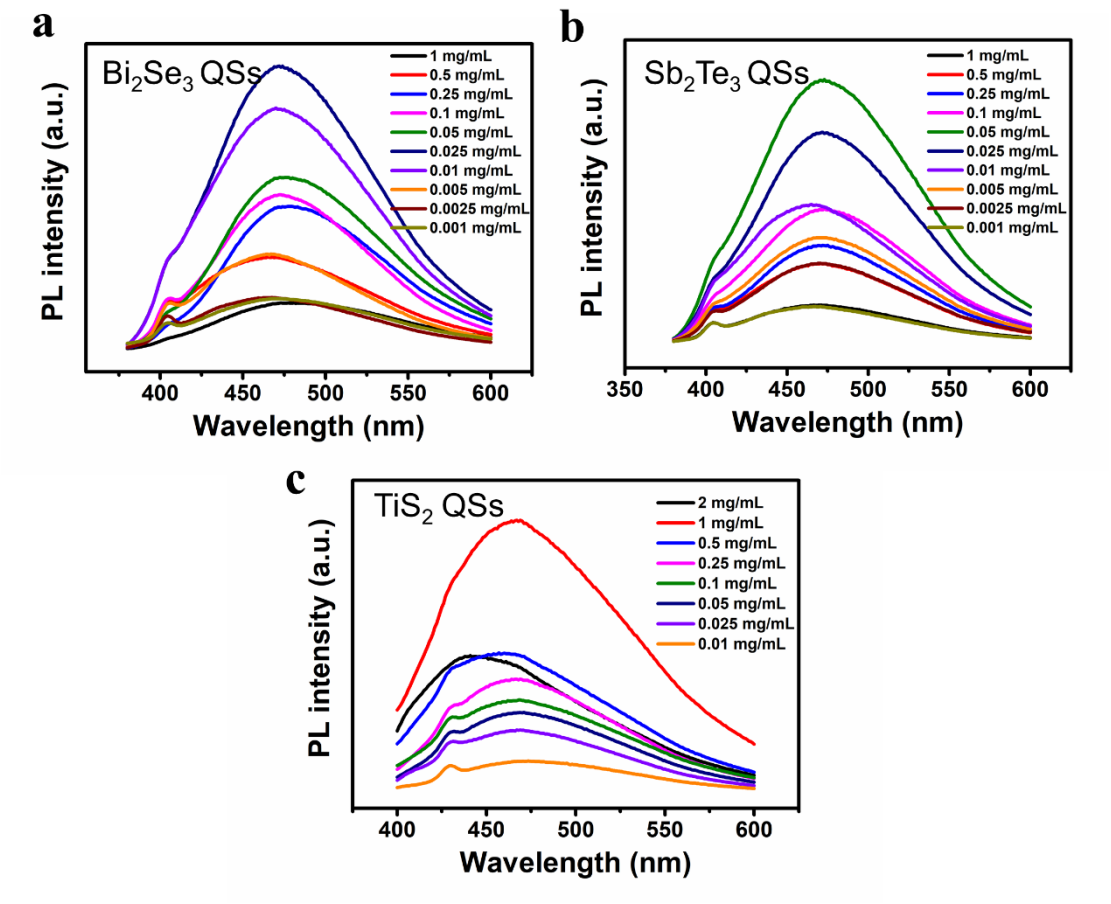

Figure S9. PL spectra of the QS/NMP dispersions at varying concentrations. (a) Bi_2Se_3 QSs, (b) Sb_2Te_3 QSs and (c) TiS_2 QSs, respectively.

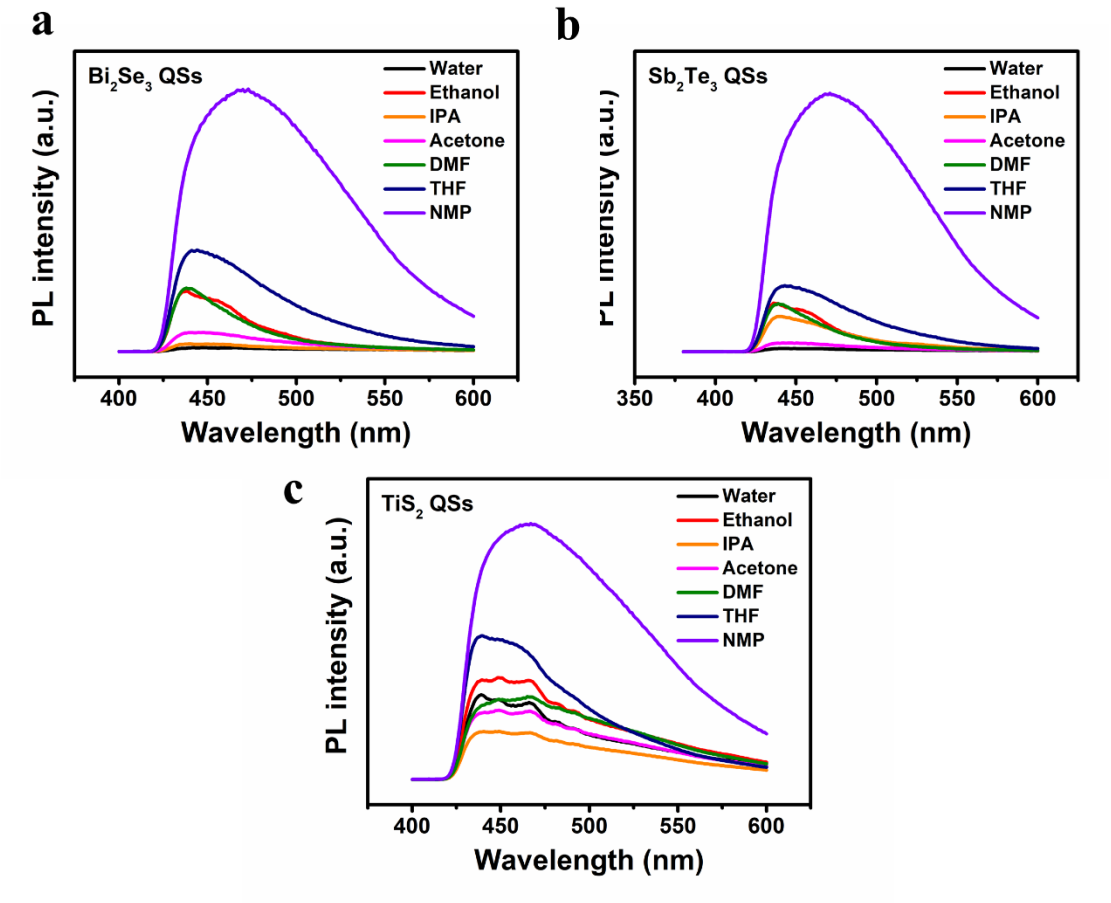

Figure S10. PL spectra of the QS dispersions in varying solvents. (a) Bi_2Se_3 QSs, (b) Sb_2Te_3 QSs and (c) TiS_2 QSs, respectively.

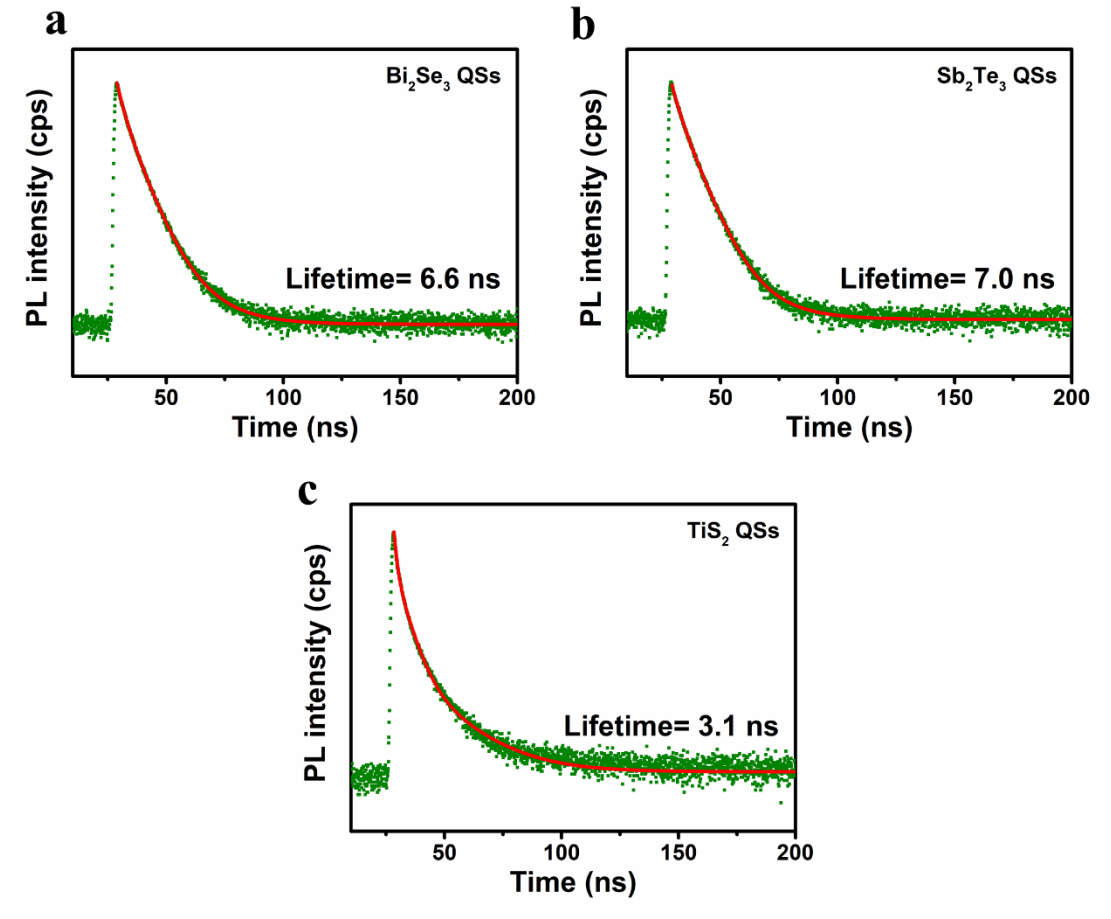

Figure S11. Time-resolved PL decay profiles of the QS/NMP dispersions upon 370 nm excitation wavelength. (a) Bi_2Se_3 QSs, (b) Sb_2Te_3 QSs and (c) TiS_2 QSs, respectively.

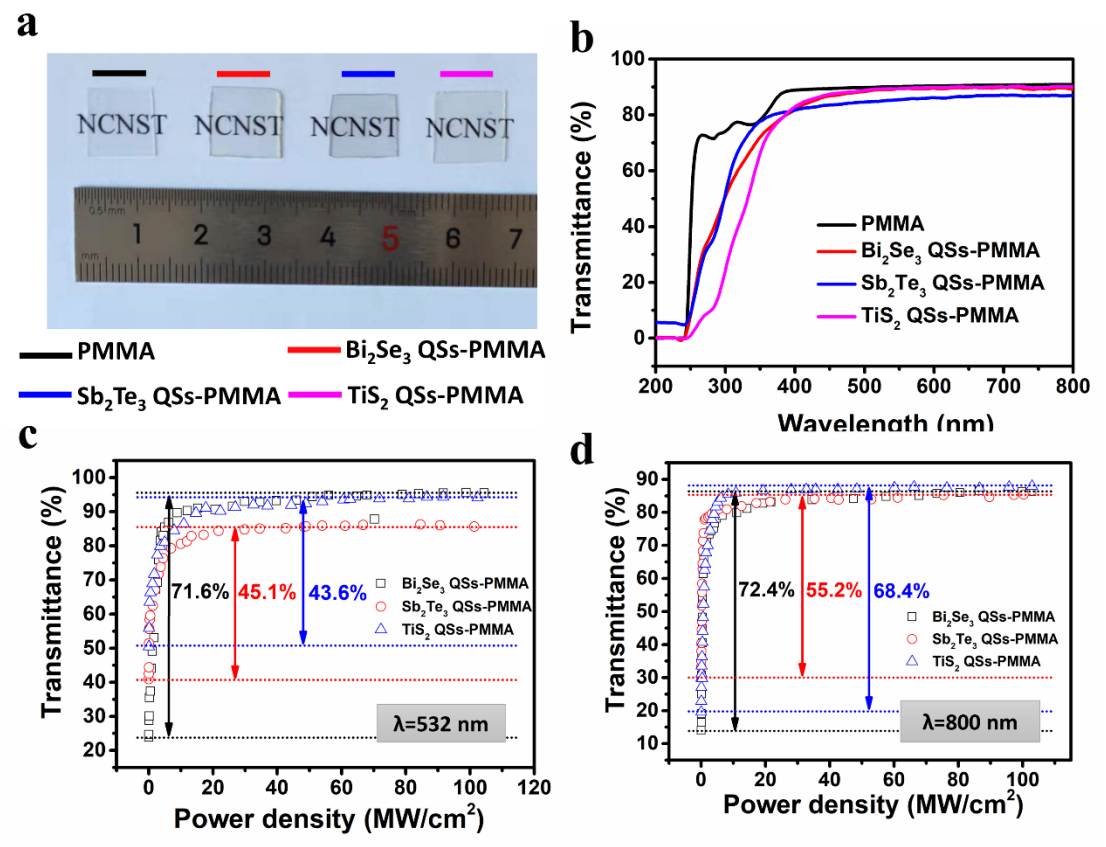

Figure S12. NLO performances of the QS solid thin films (0.1 wt%). (a) Photographs of the QSs-PMMA hybrid thin films. (b) UV-vis absorption spectra of the thin films. (c,d) Nonlinear saturable absorption curves. The incident laser beam was as follows: wavelength of (c) 532 nm and (d) 800 nm, pulse of 100 fs, and repetition rate of 1 kHz.

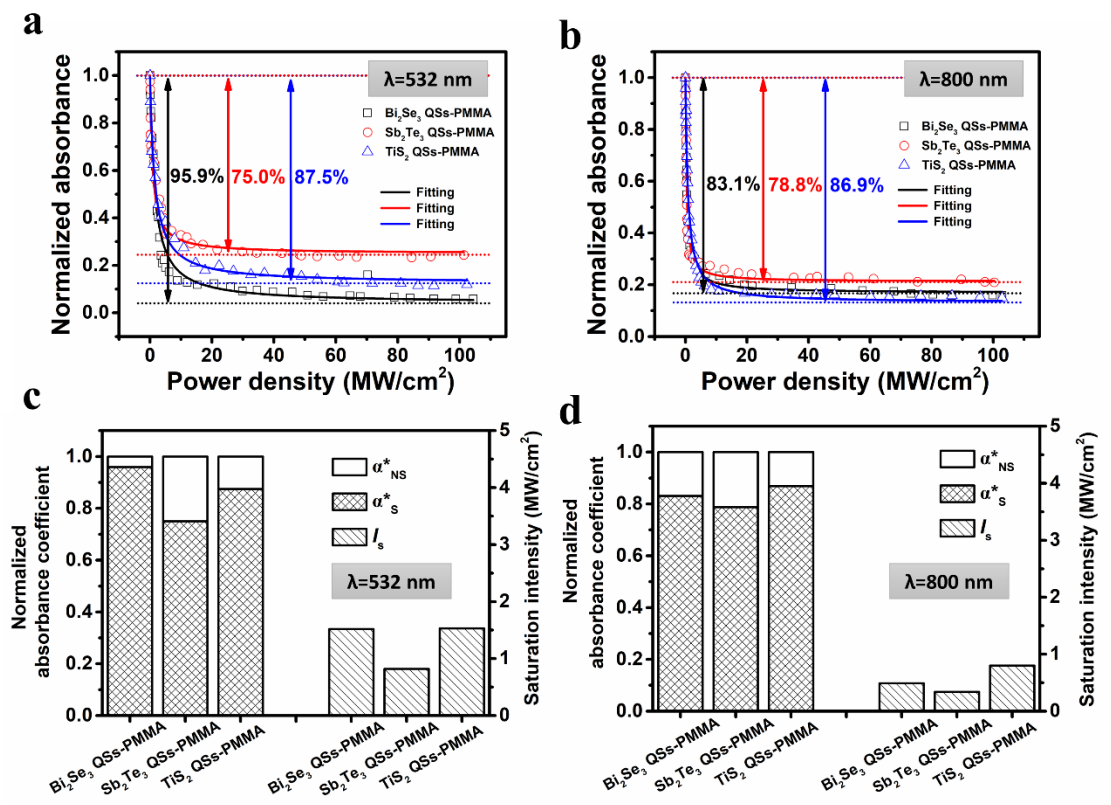

Figure S13. (a,b) Normalized absorption curves of the QS solid thin films: (a) 532 nm, (b) 800 nm. The hollow dots are the experimental data, and the solid curves are analytical fits to the data. (c,d) Plots of the normalized absorption coefficient and saturation intensity: (c) 532 nm, (d) 800 nm.

Table S1. Comparison of the NSA performances of topological insulators/semimetals from different works

Years	Materials	λ (nm)	Absolute MD (%)	I_{sat} (MW/cm^2)	References
2013	Bi_2Se_3	1568.5	41.2	101.8	S2
2013	Bi_2Se_3	800	61.2	1.012×10^4	S3
2014	Bi_2Se_3	800	3.7	41	S4
2014	Bi_2Se_3	--	3.9	12	S5
2014	Bi_2Se_3	--	5.2	580	S6
2015	Bi_2Se_3	--	3.8	25	S7
2015	Bi_2Se_3	--	4.1	26	S8
2016	Bi_2Se_3	--	3.4	31.5	S9
2016	Bi_2Se_3	1030	7.6	38.9	S10
2017	Bi_2Se_3	--	12	77	S11
2017	Bi_2Se_3	1558	39.8	90.2	S12
2018	Bi_2Se_3	1560	5	1.8	S13
2019	Bi_2Se_3	1560	15	6.59	S14
2019	Bi_2Se_3	1580	15.7	81.1	S15
2020	Bi_2Se_3	1985	9.9	--	S16
2022	Bi_2Se_3	532	71.6	1.52	This work
2022	Bi_2Se_3	800	72.4	0.49	This work
2014	Sb_2Te_3	--	3.9	106	S17
2014	Sb_2Te_3	1554	6	31	S18
2015	Sb_2Te_3	1558	13	1.25×10^3	S19

2015	Sb_2Te_3	1550	14.9	228	S20
2016	Sb_2Te_3	1568	6.2	143	S21
2016	Sb_2Te_3	1562	7.42	175	S22
2018	Sb_2Te_3	1864	38	3.3	S23
2019	Sb_2Te_3	1560	1.99	16.4	S24
2022	Sb_2Te_3	532	45.1	0.82	This work
2022	Sb_2Te_3	800	55.2	0.34	This work
2018	TiS_2	1560	8.3	--	S25
2018	TiS_2	800	62	1.21×10^3	S26
2021	TiS_2	--	5.08	10.62	S27
2022	TiS_2	532	43.6	1.53	This work
2022	TiS_2	800	68.4	0.80	This work

References

S1. Xu, Y.; Chen, S.; Dou, Z.; Ma, Y.; Mi, Y.; Du, W.; Liu, Y.; Zhang, J.; Chang, J.; Liang, C.; Zhou, J.; Guo, H.; Gao, P.; Liu, X.; Che, Y.; Zhang, Y. Robust production of 2D quantum sheets from bulk layered materials. *Mater. Horiz.* **2019,** *6*, 1416-1424.

S2. Chen, Y.; Zhao, C.; Huang, H.; Chen, S.; Tang, P.; Wang, Z.; Lu, S.; Zhang, H.; Wen, S.; Tang, D. Self-assembled topological insulator: Bi_2Se_3 membrane as a passive Q-switcher in an erbium-doped fiber laser. *J. Lightwave Technol.* **2013,** *31*, 2857-2863.

S3. Lu, S.; Zhao, C.; Zou, Y.; Chen, S.; Chen, Y.; Li, Y.; Zhang, H.; Wen, S.; Tang, D. Third order nonlinear optical property of Bi_2Se_3. *Opt. Express* **2013,** *21*, 2072-2082.

S4. Luo, Z.; Liu, C.; Huang, Y.; Wu, D.; Wu, J.; Xu, H.; Cai, Z.; Lin, Z.; Sun, L.; Weng, J. Topological-insulator passively Q-switched double-clad fiber laser at 2 μm wavelength. *IEEE J. Sel. Top. Quant.* **2014,** *20*, 1-8.

S5. Liu, H.; Zheng, X.; Liu, M.; Zhao, N.; Luo, A.; Luo, Z.; Xu, W.; Zhang, H.; Zhao, C.; Wen, S. Femtosecond pulse generation from a topological insulator mode-locked fiber laser. *Opt. Express* **2014,** *22*, 6868-6873.

S6. Dou, Z.; Song, Y.; Tian, J.; Liu, J.; Yu, Z.; Fang, X. Mode-locked ytterbium-doped fiber laser based on topological insulator: Bi_2Se_3. *Opt. Express* **2014,** *22*, 24055-24061.

S7. Guo, B.; Yao, Y.; Tian, J.; Zhao, Y.; Liu, S.; Li, M.; Quan, M. Observation of bright-dark soliton pair in a fiber laser with topological insulator. *IEEE Photon. Technol. Lett.* **2015,** *27*, 701-704.

S8. Guo, B.; Yao, Y.; Yang, Y.; Yuan, Y.; Jin, L.; Yan, B.; Zhang, J. Dual-wavelength rectangular pulse erbium-doped fiber laser based on topological insulator

saturable absorber. *Photon. Res.* **2015,** *3*, 94-99.

S9. Guo, B.; Yao, Y.; Xiao, J.; Wang, R.; Zhang, J. Topological insulator-assisted dual-wavelength fiber laser delivering versatile pulse patterns. *IEEE J. Sel. Top. Quant.* **2016,** *22*, 8-15.

S10. Li, K.; Tian, J.; Song, Y.; Liu, J.; Guoyu, H.; Xu, R.; Wang, M.; Fang, X. Bi_2Se_3 as a saturable absorber for ultrafast photonic applications of Yb-doped fiber lasers. *Opt. Eng.* **2016,** *55*, 036110.

S11. Li, K.; Song, Y.; Tian, J.; Guoyu, H.; Xu, R. Analysis of bound-soliton states in a dual-wavelength mode-locked fiber laser based on Bi_2Se_3. *IEEE Photon. J.* **2017,** *9*, 1-9.

S12. Haris, H.; Harun, S.; Muhammad, A.; Anyi, C.; Tan, S.; Ahmad, F.; Nor, R.; Zulkepely, N.; Arof, H. Passively Q-switched erbium-doped and ytterbium-doped fibre lasers with topological insulator bismuth selenide (Bi_2Se_3) as saturable absorber. *Opt. Laser Technol.* **2017,** *88*, 121-127.

S13. Li, W.; Zou, J.; Huang, Y.; Wang, K.; Du, T.; Jiang, S.; Luo, Z. 212-kHz-linewidth, transform-limited pulses from a single-frequency Q-switched fiber laser based on a few-layer Bi_2Se_3 saturable absorber. *Photon. Res.* **2018,** *6*, C29-C35.

S14. Guo, Q.; Pan, J.; Liu, Y.; Si, H.; Lu, Z.; Han, X.; Gao, J.; Zuo, Z.; Zhang, H.; Jiang, S. Output energy enhancement in a mode-locked Er-doped fiber laser using CVD-Bi_2Se_3 as a saturable absorber. *Opt. Express* **2019,** *27*, 24670-24681.

S15. Xu, N.; Ming, N.; Han, X.; Man, B.; Zhang, H. Large-energy passively Q-switched Er-doped fiber laser based on CVD-Bi_2Se_3 as saturable absorber. *Opt. Mater. Express* **2019,** *9*, 373-383.

S16. Shang, J.; Feng, T.; Zhao, S.; Li, T.; Pan, Z.; Zhao, J. Saturable absorption characteristics of Bi_2Se_3 in a 2 μm Q-switching bulk laser. *Opt. Express* **2020,** *28*, 5639-5647.

S17. Boguslawski, J.; Sotor, J.; Sobon, G.; Tarka, J.; Jagiello, J.; Macherzynski, W.; Lipinska, L.; Abramski, K., Mode-locked Er-doped fiber laser based on liquid phase exfoliated Sb_2Te_3 topological insulator. *Laser Phys.* **2014,** *24*, 105111.

S18. Sotor, J.; Sobon, G.; Grodecki, K.; Abramski, K. Mode-locked erbium-doped fiber laser based on evanescent field interaction with Sb_2Te_3 topological insulator. *Appl. Phys. Lett.* **2014,** *104*, 251112.

S19. Boguslawski, J.; Sobon, G.; Zybala, R.; Sotor, J. Dissipative soliton generation in Er-doped fiber laser mode-locked by Sb_2Te_3 topological insulator. *Opt. Lett.* **2015,** *40*, 2786-2789.

S20. Bogusławski, J.; Soboń, G.; Zybała, R.; Mars, K.; Mikuła, A.; Abramski, K.; Sotor, J. Investigation on pulse shaping in fiber laser hybrid mode-locked by Sb_2Te_3 saturable absorber. *Opt. Express* **2015,** *23*, 29014-29023.

S21. Yan, P.; Chen, H.; Li, K.; Guo, C.; Ruan, S.; Wang, J.; Ding, J.; Zhang, X.; Guo, T. Q-switched fiber laser using a fiber-tip-integrated TI saturable absorption mirror. *IEEE Photon. J.* **2016,** *8*, 1-6.

S22. Liu, W.; Pang, L.; Han, H.; Tian, W.; Chen, H.; Lei, M.; Yan, P.; Wei, Z. 70-fs mode-locked erbium-doped fiber laser with topological insulator. *Sci. Rep.* **2016,** *6*, 19997.

S23. Wang, J.; Yin, J.; He, T.; Yan, P. Sb_2Te_3 mode-locked ultrafast fiber laser at 1.93 μm. *Chin. Phys. B* **2018,** *27*, 084214.

S24. Bogusławski, J.; Soboń, G.; Zybała, R.; Sotor, J. Towards an optimum saturable absorber for the multi-gigahertz harmonic mode locking of fiber lasers. *Photon. Res.* **2019,** *7*, 1094-1100.

S25. Zhu, X.; Chen, S.; Zhang, M.; Chen, L.; Wu, Q.; Zhao, J.; Jiang, Q.; Zheng, Z.; Zhang, H. TiS_2-based saturable absorber for ultrafast fiber lasers. *Photon. Res.* **2018,** *6*, C44-C48.

S26. Ge, Y.; Zhu, Z.; Xu, Y.; Chen, Y.; Chen, S.; Liang, Z.; Song, Y.; Zou, Y.; Zeng, H.;

Xu, S.; Zhang, H.; Fan, D. Broadband nonlinear photoresponse of 2D TiS_2 for ultrashort pulse generation and all-optical thresholding devices. *Adv. Opt. Mater.* **2018,** *6*, 1701166.

S27. Shang, X.; Guo, L.; Zhang, H.; Li, D.; Yue, Q. Passive mode-locked Er-doped fiber laser pulse generation based on titanium disulfide saturable absorber. *Front. Inf. Technol. Electron. Eng.* **2021,** *22*, 756-766.